Forming Uniform Deuterium Hydride and Deuterium–Tritium Layers in Shells

*D. N. Bittner** *B. Kozioziemski* *J. Pipes***
T. P. Bernat *S. Letts* *M. Saculla*
*J. Burmann** *E. R. Mapoles* *J. D. Sater**
G. W. Collins *E. Monsler** *W. Unites*

Introduction

Smooth and uniform, 50- to 300-μm-thick deuterium–tritium (DT) layers on the interior of 1- to 3-mm-diam spherical capsules are required for ignitable inertial confinement fusion (ICF) targets for the National Ignition Facility (NIF).[1] One way to form such layers is to initially freeze DT to an anisotropic, multicrystalline solid inside a capsule and then allow the tritium-decay volumetric heat generation, $Q_{DT} = 0.05$ W/cm^3, to symmetrize the layer. Volumetric heating causes the thicker regions of the solid to have a higher temperature, thus higher vapor pressure. The result is a redistribution of the solid until the inner DT surface is isothermal. The time constant for such redistribution (when no ^{3}He is present) is $\tau_0 = H_s\rho / Q_{DT} = 27$ min, where H_s is the heat of sublimation (1580 J/mole), and ρ is the density (0.0503 moles/cm^3) (Ref. 2). If bulk heating were the only factor controlling the layer profile, DT would form a uniform spherical layer inside an isothermal spherical capsule. However, crystal surface stiffness contributes to the final layer shape. The surface smoothes until the thermal energy associated with material redistribution is comparable to the surface energy gained in having to form a higher-energy viscinal surface.[3] The surface structure of a multicrystalline DT film is a function of the DT bulk heating rate and the distribution of crystallite sizes and orientations, which are determined by the initial nucleation and growth.[4]

Several implosion hydrodynamics issues of cryogenic targets can be investigated with deuterium hydride (HD) or deuterium (D_2) without the hazards of handling high-pressure tritium. To generate bulk heat for mass redistribution without tritium radiation, we pump the collisionally induced, infrared (IR) vibration–rotation band. We regulate the solid volumetric heating rate Q_{IR}, thus the redistribution rate $1/\tau_{IR}$, and surface roughness by controlling the incident IR intensity. We have measured laser-power-limited $1/\tau_{IR}$ (thus Q_{IR}) in HD up to 10 times higher than the DT value. The maximum Q_{IR} for hydrogen isotopes is limited by the vibrational relaxation time to $Q_{IR} \approx 1000\ Q_{DT}$.[5] Such large Q_{IR} values enable us to control the hydrogen layer profile and to explore the redistribution process of laser-heated solids.

Forming Uniform HD Layers in Shells

Experimental Overview

We previously measured redistribution time constants τ_{IR} from IR illumination of both solid HD and D_2 at several different wavelengths versus incident IR flux to determine Q_{IR}.[6,7] Our redistribution experiments showed that the illumination of a solid sample with IR radiation resulted in redistribution of the solid in a manner analogous to that seen with tritium heat generation in DT. In a second series of experiments using a similar experimental design, but with a larger sapphire cell, we investigated the surface roughness of a layer formed by illuminating the solid with IR. The illumination pattern of the IR was found to have significant influence on layer shape. The resultant phase-shifting interferometric analysis revealed that surface perturbations with spatial extent greater than the layer thickness have amplitudes that decrease with increasing volumetric heating. The minimum roughness achieved at a given volumetric heating rate was found to depend on the nucleation and subsequent crystal growth during freezing. Both of these experiments

*Schafer Corporation, Livermore, CA
**Allied Signal Inc., Livermore, CA

were effectively one dimensional. A laser beam made one pass coaxially along the inner bore of the cell, and measurements were made by looking through the side of the container or coaxially along the bore of the cell. In the present experiments, we generated 4π illumination of HD inside a 1-mm–outside-diameter (o.d.) spherical capsule and observed the evolution of a uniform solid layer as a function of time and IR intensity.

Experimental Design and Layout

Several issues needed to be addressed in designing our experiments. The first issue was the choice of capsule material. The goal was to heat the HD (D_2 or DT) and not the plastic shell. Therefore, it was important to minimize the amount of IR absorption (heating) by the capsule. Standard plasma polymer, $CH_{1.3}$, used in current Nova experiments has several absorptions overlapping the absorption band for both D_2 and HD. Thus, it would be difficult to redistribute HD or D_2 in shells made of this material. The absorption bands are primarily CH and OH stretch modes. A broadband loss of transmission, which may result from IR scattering, also extends over the entire spectral range of measurement (400 to 5125 cm^{-1}). Therefore, we explored alternatives and found that a CD plasma polymer made with deuterated p-xylene monomer and D_2 flow gas does not have corresponding strong CH absorption lines and has good broadband transmission as well. Furthermore, whereas the OH absorption band increased with time in air, it is controlled by keeping the shell in a dry box. CD plasma polymer was the shell material used for our experiments (Figure 1).

A second issue was the technique for generating uniform IR illumination. The experiments on surface roughness showed that diffuse illumination was necessary to reduce laser-induced coherence effects.

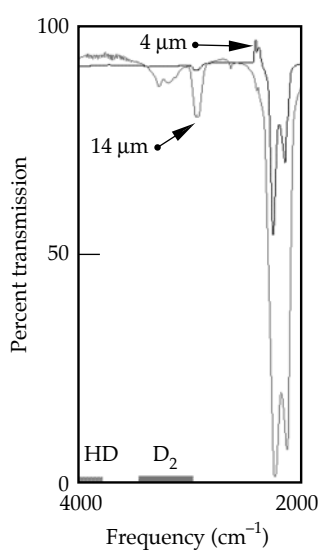

FIGURE 1. IR transmission spectra of 4-µm and 14-µm-thick CD plasma polymer films. Overlapping absorption-band ranges for HD and D_2 are indicated along the bottom of the plot. (08-00-1298-2502pb01)

Calculations showed that illumination uniformity to better than 99% could be achieved[8] by using an integrating sphere. The integrating sphere for our experiments was a vacuum-tight enclosure made from aluminum, with four window ports and an Infragold coating[9] on the inner surface. The Infragold surface is greater than 96% reflecting at wavelengths of interest.

Although we did not perform a systematic study of surface roughness as a function of Q_{IR}, the smoothest surfaces were generated at $Q_{IR} \approx 200$ mW/cm^3. Using this value, we can estimate the IR power requirements for the integrating sphere. The volumetric heating rate is related to IR intensity by $Q_{IR} = \alpha I$, where α is the absorption coefficient [α(HD) ≈ 8/cm], and I is the intensity. The requisite volumetric heating rate is produced by injecting sufficient IR into the integrating sphere to produce the required intensity $I_0 = Q_{IR}/\alpha$. For weakly absorbing layers, $I \approx I_0$, the incident intensity. The capsule is small compared to the integrating sphere, so that most of the power losses occur at the integrating sphere wall and through the viewports. The injected power only needs to be sufficient to compensate for integrating sphere losses of about 4%. This results in a linear relation between laser power and incident intensity, $P_{IS} = 0.04 I_0 A_{IS}$, where P_{IS} and A_{IS} are the injected IR power and surface area of the integrating sphere, respectively. Thus, an intensity of $I_0 =$ 25 mW/cm^2 incident on the 1-mm-o.d. capsule in the center of a 25-mm–inside-diameter (i.d.) integrating sphere requires 21 mW of IR.

Finally, asymmetries in the solid layer, arising from perturbations in the thermal environment caused by the fill tube, needed to be minimized. The fill tube essentially acts as a cooling fin on the shell. Thermal conductance through the fill tube is greater than that of the surrounding helium exchange gas. The difference causes the shell area around the fill tube to be cooler than the rest of the capsule, resulting in formation of a thicker layer in this region. Various means of attaching a fill tube to the capsule were investigated and modeled using the finite element code COSMOS. The final design involved overcoating a composite-shell/fill-tube mandrel with plasma polymer. The resulting capsule was nominally 1-mm o.d. with a 10-µm-thick wall seamlessly attached to a 1- to 2-mm-long by 30-µm-o.d. plasma polymer fill-tube extension.[10]

Figure 2 shows a sketch of the experimental layout. A CD shell containing HD was placed in the center of a 25-mm-i.d. integrating sphere filled with roughly 0.5 Torr of helium exchange gas. The fill line consisted of three sections: a 0.82-mm-long CD tube attached to a 5-mm-long glass tube, which was, in turn, attached to a stainless steel tube. The stainless tube extended through the integrating sphere wall. To minimize IR absorption in the fill line, the glass tube was gold coated. The shell containing HD was illuminated through one pair of viewports by an IR laser beam,

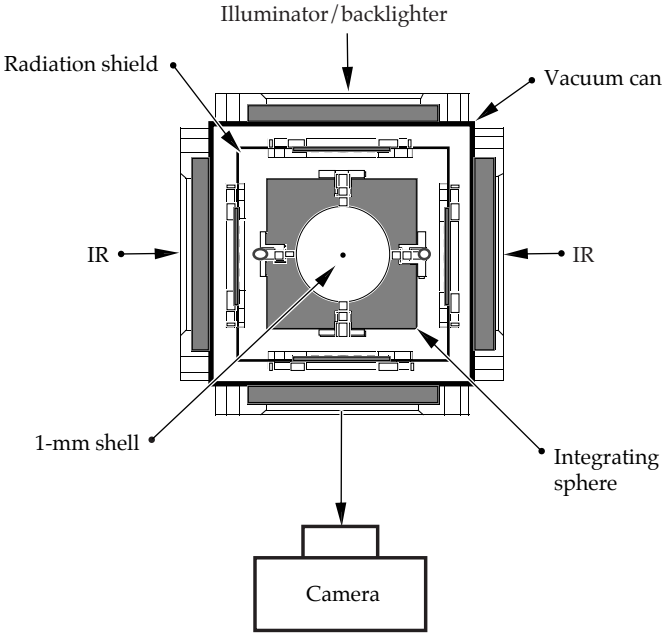

FIGURE 2. Experimental layout indicating the viewing axis and IR injection axis. Sapphire ball lenses on the integrating sphere ports spread the IR beam in an $f/1$ cone. (08-00-1298-2503pb01)

and the layer was monitored along a second orthogonal axis by backlighting the capsule through one port and using a Questar microscope on the opposite port for viewing. Images were acquired periodically during layer formation using a Photometrics 1317 × 1035 array charge-coupled device (CCD) camera attached to the microscope. Real-time monitoring of the layer was done with a Cohu camera mounted on the microscope eyepiece port. The integrating sphere was thermally and mechanically attached to the cold tip of a helium flow cryostat.

Data Collection and Analysis Procedures

To determine the bulk heating rate, we measured the redistribution time constant τ_{IR}. This measurement was accomplished by filling the capsule with HD, rapidly cooling to approximately 15 K to freeze the HD, and then turning on the IR illumination and collecting images of the evolving layer with time. The HD thickness was typically small near the top of the shell, but grew exponentially with time to form a uniform layer. The exponential time constant is related to the volumetric heating rate by $\tau_{IR} = H_s\rho / Q_{IR}$.

Roughness of the inner solid surface was determined by performing a fast Fourier transform (FFT) analysis of the bright band in the CCD camera images. The bright band can be understood by performing a ray trace[11] through a 1-mm-o.d. shell containing a uniform layer inside an integrating sphere with 4-mm-o.d. ports. The HD-filled capsule acts as a weak, negative lens, resulting in light near the edge of the shell being refracted out of the field of view. Rays internally reflected off the inner solid surface do not leave the field of view and travel through the shell and integrating sphere viewport to the collection optics. Figure 3a shows a closeup view of a bundle of rays incident on the capsule. Figure 3b is an expanded view, showing the rays exiting the integrating sphere through a viewport. Bundles of rays incident on the shell at the largest incident angles consistent with our optical arrangement were traced and found to produce the same bright band.

Refraction also affects the determination of layer thickness. Typically, layer thickness is determined by acquiring an image with the CCD camera, measuring the distance from the bright band to the edge of the shell in pixels, comparing that to the measured distance across the diameter of the shell, also in pixels, and scaling pixels to micrometers using the shell diameter previously determined by standard characterization techniques.[12] If the microscope is focused at the center plane of the shell, then by using this method, one assumes that the rays from the bright band extrapolate in a straight line back to the center of the shell. Figure 3a shows a dashed line extrapolating the rays to the center plane of the shell. The measured, or apparent, layer thickness determined from a camera image is less than the actual layer thickness by the difference between the dashed line and the inner solid surface. To estimate the actual layer thickness, a simple model was generated to calculate both apparent and actual layer thicknesses inside a 10-μm-thick, 1-mm-o.d. plastic shell. The results in Figure 4 show that refractive effects have a significant impact on the measurement of thin layers, especially those less than 100 μm. For example, a 100-μm-thick layer would appear to be only 45 μm thick on the image.

Once the images were shot and stored, the objective of the experiment was to extract an estimate of surface roughness from the stored data. We previously

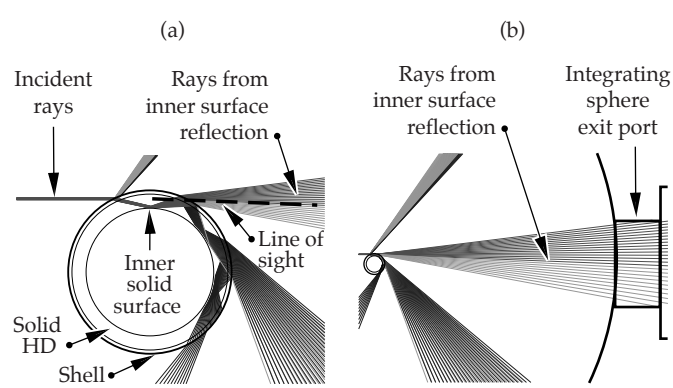

FIGURE 3. (a) Ray trace plot showing the reflection of light off the inner solid surface. (b) Most such light passes out of the integrating sphere through the viewport. (08-00-1298-2504pb01)

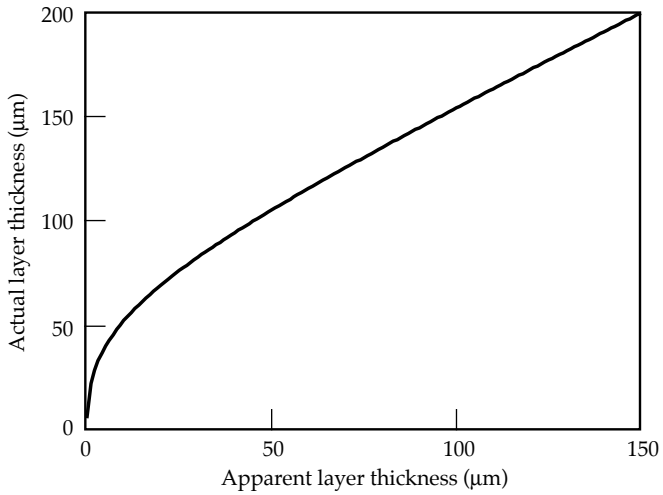

FIGURE 4. Apparent versus actual layer thickness inside a 1-mm-o.d. shell. (08-00-1298-2505pb01)

developed software that locates the surface of the solid in the image.[3] The resultant 1D estimate of solid thickness variations are Fourier transformed to estimate the power spectrum of perturbations on the solid layer.

The software begins by taking an estimate of the center of the bright band in the image and drawing a ray from the center to the edge. At 1-pixel increments along the ray, the intensity is estimated by fitting a plane to the four neighboring pixel values and interpolating to obtain the intensity at the point on the ray. This procedure is done for a series of rays offset by some given angular increment to generate an image of the target in polar coordinates. Each column in the image is then processed to locate the light-to-dark transition associated with the inner edge of the solid. Estimates of the locations of the edge of the bright band are averaged to give a new value of the center of the bright band, and the image is reprocessed until the estimates converge.

A large step in intensity occurs at the inner edge of the solid. Refraction at the inner edge creates intensity minima in the spherical geometry, which are located using an algorithm to find the minima in each ray. Minima are sorted by depth for each ray to give an array of locations as a function of angle for each feature. The profiles can be Fourier transformed and the results used to calculate power spectra for the surfaces. Because we do not locate the shell edge, we do not determine the offset of the inner surface from the capsule (Fourier mode 1), but fit Fourier modes 2 through 128.

Results and Discussion

Layers grown by the rapid-cooling technique typically result in rough, multicrystalline surfaces. Figure 5 shows the evolution of one of the rough layers in which the volumetric heating rate was ~250 mW/cm^3 (or 5 Q_{DT}). The layering process began by performing a controlled liquid fill. Once sufficient liquid was inside the capsule (Figure 5a), the temperature was quickly lowered to freeze the solid (Figure 5b). The randomly grown solid was then illuminated with IR radiation, and redistribution of the solid was recorded with time. Figure 5c shows the resultant layer.

To improve the quality of the inner solid surface, we developed a second technique. The technique is currently performed by manually entering the temperature into a temperature controller while viewing the layer evolution on a monitor. To grow higher-quality layers, we freeze the HD, inject IR radiation into the integrating sphere, raise the temperature of the capsule until the solid just finishes melting, and slowly lower the temperature in approximately 0.005-K steps until freezing onset occurs, at which point the temperature is no longer lowered. If solidification appears to stop, then the temperature would be lowered in 0.005-K steps until a uniform layer forms. Images of the evolving layer were recorded with time. Figure 6 shows an approximately 200-μm-thick layer grown by this technique. Figure 7 is the power spectrum for the solid layer in Figure 6d. The resultant rms for this layer is 2.24 μm. This technique is slightly different from the slow-growth technique used for DT layers, which is

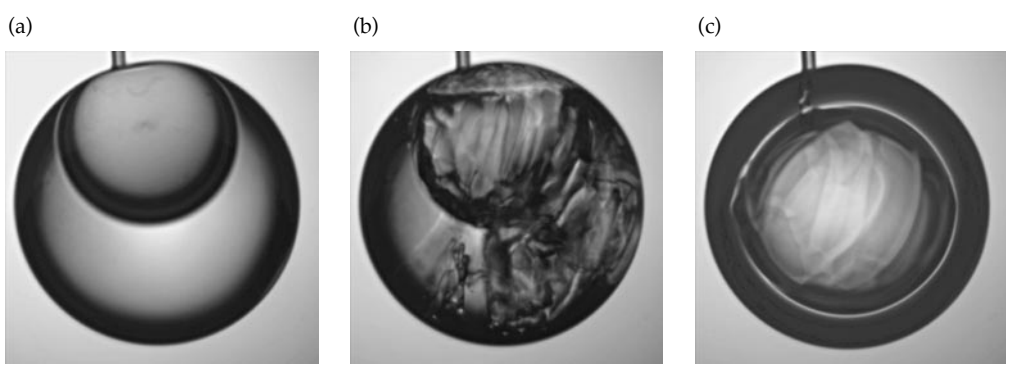

FIGURE 5. To generate a layer from the solid, (a) the capsule is filled with liquid at 16.6 K, (b) the temperature is lowered to 15.8 K to form solid, and (c) upon application of IR, the solid redistributes to form a layer. Layers typically have a rough surface, even after 16 hr in this case. (08-00-1298-2506pb01)

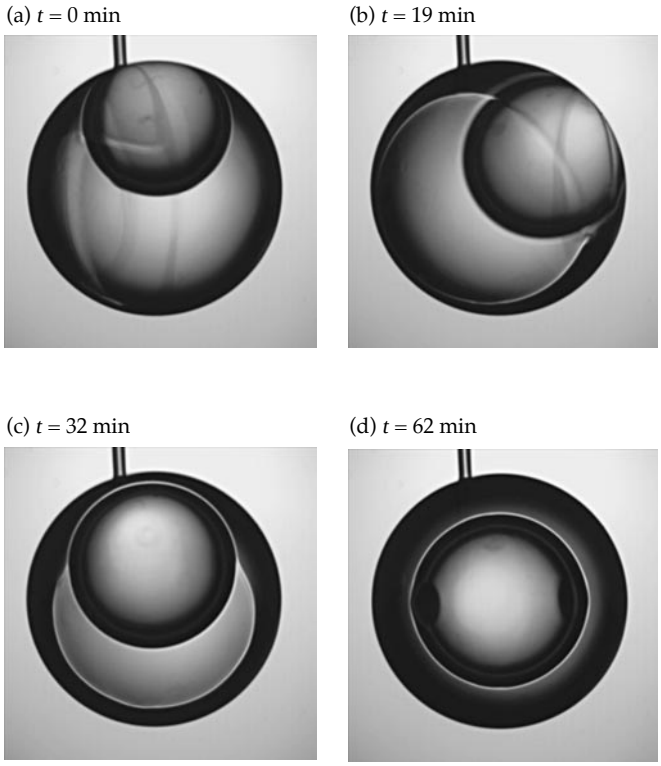

FIGURE 6. In an improved layering technique, IR is continually applied to the capsule. The capsule is warmed to the liquid phase (16.6 K) and slowly cooled until (a) solid starts forming. The temperature is then held constant during the solidification process (b through d). (08-00-1298-2507pb01)

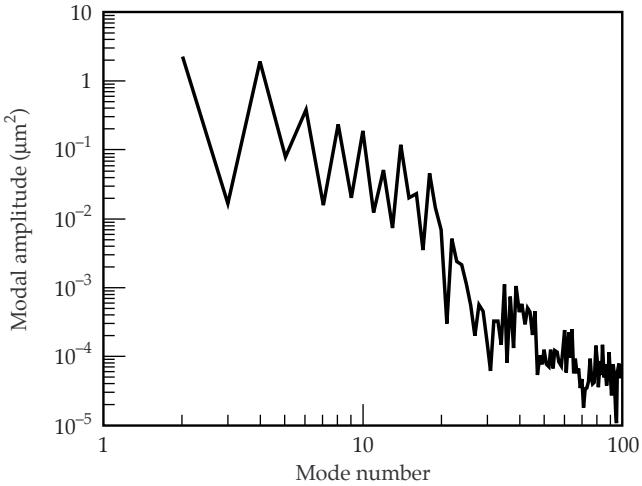

FIGURE 7. Power spectrum for the layer shown in Figure 6d. The rms value of this layer is 2.34 μm. (08-00-1298-2508pb01)

discussed later in this article. Because DT is a mixture, there is no triple point as in a single-component system (D_2), but a three-phase region. The slow-growth technique cools the DT slowly through this region.

Laser power and temperature stability affect the growth of the solid. Higher-quality layers were formed when the temperature was controlled to at least ±5 mK under stable laser power. The impact of the laser is twofold. In addition to generating a given volumetric heating rate, the absorbed energy also raises the temperature of the solid. Variations in laser power cause both volumetric heating rate and temperature variations. Large temperature fluctuations cause the HD to melt and freeze too rapidly, resulting in rough layers. When both systems were stable, it typically took about one hour for layer completion.

As shown in Figures 5c and 6d, some features in the layers are similar in these images. One is a "bump" (or flat spot) near the fill tube. The fill tube has higher thermal conductivity than the surrounding helium exchange gas, producing a cold spot at the fill-tube–shell junction and resulting in a thickening or bump in the layer. The only way to remove this feature is to eliminate the fill tube. The second pair of features, seen at the shell equator, is due to the IR injection method. The IR is injected along an axis through the equator of the shell, resulting in more intense illumination than from the rest of the integrating sphere. The locally warmer areas result in thin spots in the layer. Such features can be removed by alternative injection techniques, such as shaping the beam, inserting a beam block in front of the shell, or, more easily, by initially directing the beam to miss the shell instead of passing through it.

Figure 8 shows a 180-μm layer produced by directly injecting the beam into the integrating sphere. For this arrangement, the sapphire balls were removed, and one beam was injected off-axis at an angle of 11° through the integrating sphere window. Such injection permitted the ~2.5-mm-diam beam to pass through the window, miss the shell, and hit the integrating sphere wall. A thickening of the layer near the fill tube can still be detected, but the thin spots at the equator seen in the previous arrangement are gone. Layers grown using IR illumination are comparable to DT layers grown by the slow-freeze technique. Figure 9 shows the power spectrum for this layer and, for comparison,

FIGURE 8. Layer formed by direct injection of the IR laser beam after removal of sapphire ball lenses. Thinning of the layer at the capsule equator is no longer evident. (08-00-1298-2509pb01)

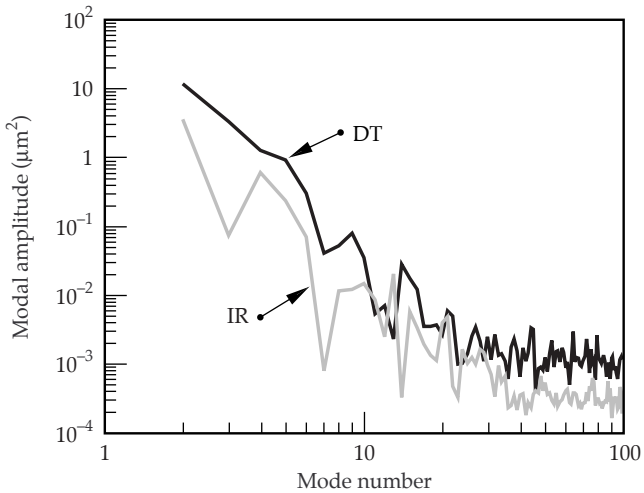

FIGURE 9. Power spectrum for the layer shown in Figure 8 along with a DT layer of comparable thickness. (08-00-1298-2510pb01)

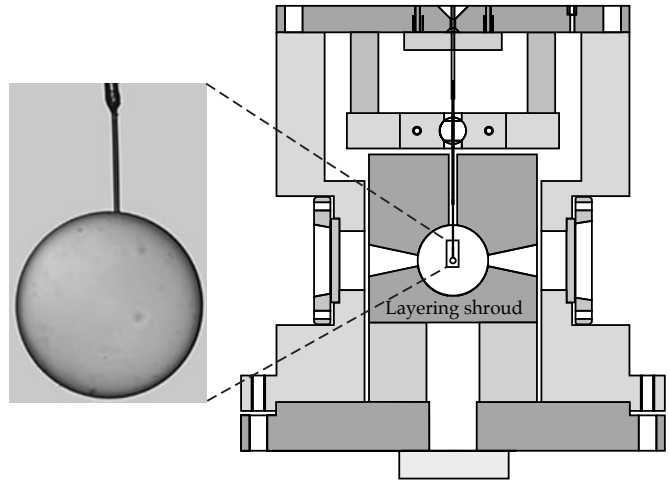

FIGURE 10. Layering occurs in a spherically symmetric geometry. (08-00-1298-2511pb01)

a power spectrum for the ~150-μm-thick DT layer grown by the slow-freeze technique. The IR-generated layer has the same general modal shape as the DT layer.

Forming Uniform DT Layers in Shells

Experimental Overview

We also conducted experiments on a mixture of approximately 25% T_2, 25% D_2, and 50% DT, referred to as DT. The sample was introduced as a liquid in the normal rotational state. Throughout the experiment, $J = 1$ to $J = 0$ conversion occurs continuously, but no measurements were made of rotational content. Our experimental setup, data collection, and analysis were similar to procedures described in a recent paper.[13] The main difference between this experiment and the previous experiment was the replacement of a cylindrical sapphire sample cell with a series of 1-mm-diam plastic shells with 10- to 20-μm-thick walls.

Experimental Design and Layout

A DT ice surface conforms to the isotherms shaped by the surrounding layering shroud. Because a smooth, spherical shape was desired, the layering shroud was a 25.4-mm-diam hollow sphere made of OFHC copper, shown in Figure 10. This shroud provided a constant-temperature, spherical boundary condition. The cell was filled with DT liquid via a fill tube, as shown in Figure 10. A few Torr of ^{4}He gas inside the sphere caused conductive cooling of the plastic shell. The cavity was cooled from the bottom to minimize convection inside the sphere. This design allowed us to study layering in a system quite similar to that required for many ICF target designs.

The plastic shell was placed at the center of the hollow sphere. A pair of 3-mm holes and a pair of 5-mm holes were bored in the layering shroud on perpendicular axes to provide a view of the sample cell. The holes had negligible effect on the spherical isotherms. The shroud was placed inside of a vacuum-sealed secondary container.

Temperature was measured by two calibrated germanium resistance thermometers (GRTs) placed on the top and bottom of the copper cavity. The mean value of the two GRTs was the reported temperature. Temperature stability was better than 2 mK over a period of hours, and temperature resolution was 1 mK. Calibration was checked by measuring the triple point of our D_2 sample, which was 18.72 K, compared to 18.73 K reported for nD_2.[14]

Because the IR and beta layering experiments were of similar design, we were able to share resources. For example, the shells used for both experiments were made from CD plasma polymer. In addition, thermal and ray trace modeling, discussed previously, were applicable to both experiments.

Results and Discussion

Figure 11 shows the evolution of the temperature and rms surface-roughness σ during the course of an experiment carried out on a 3-day-old sample of DT. The value of σ was calculated from modes 2 through 128. In this experiment, we cooled slowly through the triple point at a constant rate of 0.5 mK/min, until the set-point temperature of 19.78 K was reached. The temperature was then held constant for a period of time. The DT layer grows during the temperature ramp,

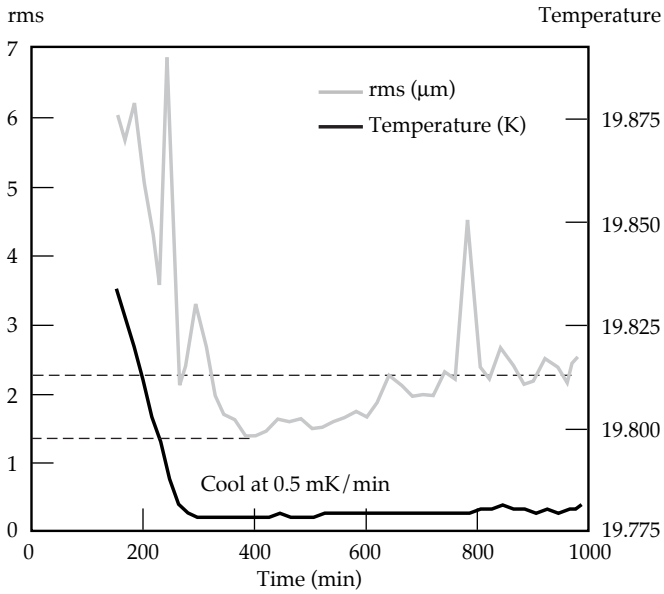

FIGURE 11. The layer smoothes to a minimum value and then roughens with longer times. (08-00-1298-2512pb01)

with a single growth front that begins near the top of the shell. The crystal growth front converges at the bottom of the shell to complete the layer. After formation, $T = 19.78$ K, time = 295 min, and $\sigma = 2.65$ μm. The layer continues to smooth, reaching a minimum σ of 1.15 μm at about 383 min. Afterwards, the layer roughens; however, such behavior is not well understood.

Figure 12 shows the power spectral density for the layer at 400 and 1000 min. The layer at 400 min is smoother at all mode numbers, except perhaps at a singular point at mode 7. Most of the difference between the two layers occurs in modes 2 to 4.

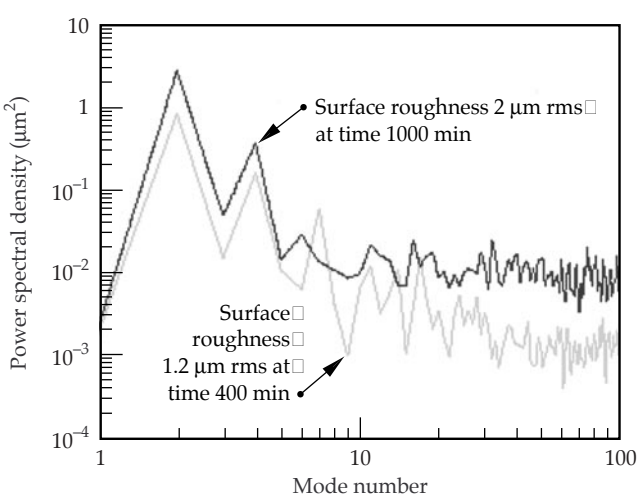

FIGURE 12. An increase in roughness over time after minima is largely due to effects at modal numbers between 2 and 4, although the largest relative increase occurs above mode 20. (08-00-1298-2513pb01)

The freezing rate has a strong effect on layer smoothness. In Figure 13, σ is plotted for a series of 210-μm layers formed at different freezing rates. For rates slower than 3 mK/min, a dramatically smoother layer is produced. At faster freezing rates, the DT nucleates several small crystals instead of growing with a single front. Layers with several distinctly observable crystals are significantly rougher than those formed from a single nucleation site.

Our data indicate that σ increases with decreasing layer thickness. Figure 14 shows a collection of all our

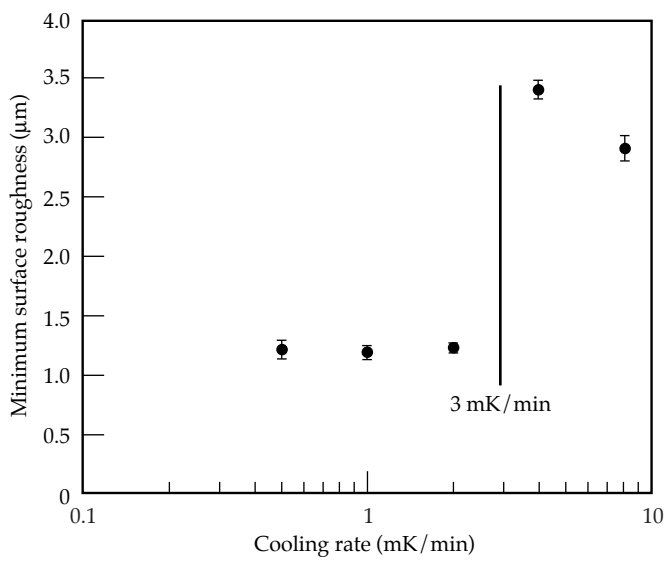

FIGURE 13. Best surface roughness achieved for a series of 210-μm layers created with different cooling rates through the triple point of DT. (08-00-1298-2514pb01)

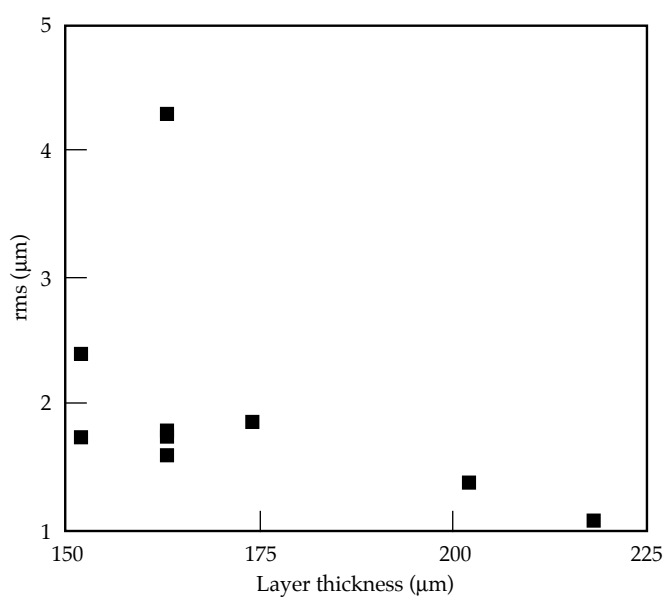

FIGURE 14. Thinner ice layers have a larger σ. (08-00-1298-2515pb01)

layering data with cooling rates between 1 and 2 mK/min and layer thicknesses between 150 and 225 μm. The 4.2-μm point was for a layer formed at the upper end of the cooling rate. Figure 15 shows the power spectral density for a 152-μm layer and a 220-μm layer. The thicker layer is substantially smoother at all mode numbers. This result could be due to the observed relative ease by which thick layers nucleate, compared to thin layers. A contributing factor is the increase in variation of temperature near the ice–gas interface with thicker layers. That is, $\delta T_{\text{bump}} = Qh\delta h_{\text{bump}}/k$, where δT is the variation from the average temperature at the ice–gas interface, and δh is the variation from the mean ice thickness.

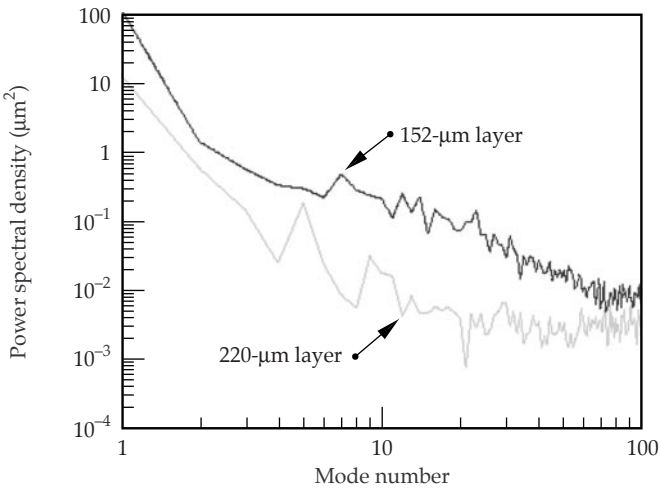

FIGURE 15. Power spectral density plots indicate that a large amount of excess power for the thinner layers is in the middle part of the modal spectrum. (08-00-1298-2516pb01)

The second type of distinct experiment we carried out was a slow, continuous freeze through the triple point of DT to a point well below the triple point. Figure 16 shows the temperature versus time evolution and σ versus time plotted on the same graph. Once again, we observe that the surface reaches a minimum roughness, then at later times becomes quite rough as the layer continues to cool.

Layers at temperatures below $T_{\text{TP}} - 0.5$ K are typically rougher than layers produced just below T_{TP}. Currently, NIF ignition target designs contain 80-μm-thick DT layers at 18 K inside a 2-mm-o.d. capsule. Our best DT layers are produced just below T_{TP} at about 19.7 K. Gas density inside the capsule is $\rho_{\text{gas}} = 0.7$ mg/cm^3, instead of the specified $\rho_{\text{gas}} = 0.3$ mg/cm^3, and would therefore change the convergence of the ignition capsule design.

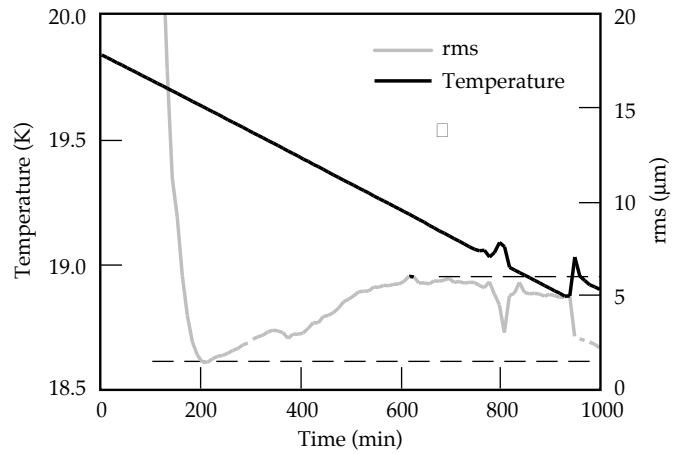

FIGURE 16. With a continuous freeze, the layer reaches a minimum σ early and then degrades. (08-00-1298-2517pb01)

Surface Roughness Model

The equilibrium ice layer minimizes the total free energy at constant volume. The thermal gradient resulting from tritium decay heating favors uniform layers; however, the anisotropic surface energy favors facets. The curved shell geometry prevents the layer from having a single low-energy facet exposed along the entire surface, and any recrystallization to reorient the surface is limited by grain-boundary energy. We can model each of these energies to understand the layer roughness.

The total free energy per unit length is expressed as

$$E_{\text{T}} = \int_A C\rho T dA + \sum_{i=1}^{n} \gamma_{\text{s}}^{i} L_i + \sum_{i=1}^{n} \gamma_{\text{gb}}^{i} t_i \ , \qquad (1)$$

where C is the specific heat, ρ is the ice density, γ_{s}^{i} is the orientation-dependent surface energy, L_i is the length of the crystal facet, γ_{gb}^{i} is the grain-boundary energy, t_i is the grain-boundary length, and A is the bulk ice area perpendicular to the cylindrical axis.

The c-facet for solid deuterium was determined to have $\gamma = 6 \times 10^{-3}$ J/m^2 (Ref. 15). The best estimate for γ_{gb}^{i} is 0.6×10^{-3} J/m^2, or 10% of the surface energy.[16] Using a 1D heat-flow model for a layer with cylindrical geometry and n regular low-energy facets, as shown in Figure 17, we find that $n = 53$ minimizes the free energy for a 210-μm layer. The corresponding rms surface roughness is 0.15 μm. The model predicts that rms surface roughness decreases with increasing layer thickness out to 300 μm for a 1-mm shell, consistent with the data in Figure 14.[17] The magnitude of the predicted roughness is smaller by a factor of 10 than the data because of the highly idealized nature of the model. A more detailed model should include multiple crystal orientations and grain-boundary energies.

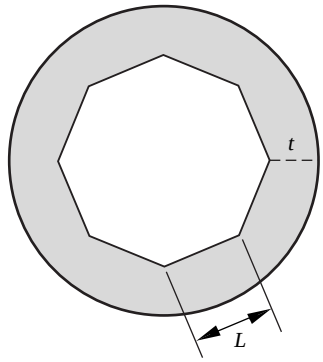

FIGURE 17. Simplified crystal geometry in a DT ice layer. Length of a single crystal facet is denoted as L, and t is crystal thickness. (08-00-1298-2518pb01)

Summary

We have presented the first results from beta layering in 1-mm plastic shells with fill tubes. Our best beta layers have a roughness as small as 1.2 μm rms for a 210-μm-thick ice layer. Layer smoothness depends on cooling rate as well as layer thickness. Our best DT ice layers are formed when freezing through the triple point is slower than 3 mK/min for 210-μm layers. Data and simple calculations indicate that thinner layers are rougher layers.

We have developed a technique to redistribute and smooth hydrogen (D_2, HD, DT, etc.) layers for ICF by slow solidification with simultaneous pumping of the rotation–vibration absorption bands of the solid. Relatively uniform layers can now be grown with a surface roughness comparable to that of DT. Crystals formed during a quick freeze to the solid phase are not readily smoothed by IR heating. Solid layers slowly grown from the melt were much smoother.

Notes and References

1. J. Lindl, *Phys. Plasmas* **2**(11), 3933–4024 (1995); E. M. Campbell and J. C. Browne, *Science* **271,** 130–132 (1996).
2. A. J. Martin, R. J. Simms, and R. B. Jacobs, *J. Vac. Sci. Technol. A* **6**(3), 1885 (1988); J. K. Hoffer and L. R. Foreman, *Phys. Rev. Lett*. **60**, 1310 (1988); T. P. Bernat, E. R. Mapoles, and J. J. Sanchez, *ICF Quarterly Report* **1**, 57, Lawrence Livermore National Laboratory, Livermore, CA, UCRL-LR-105821-91-1 (1991).
3. G. W. Collins et al., *ICF Quarterly Report* **3**, 81, Lawrence Livermore National Laboratory, Livermore, CA, UCRL-LR-105821-93-3 (1993).
4. *Solids Far From Equilibrium*, C. Godreche, Ed. (Cambridge University Press, Cambridge, 1992). In this article, we ignore effects from ^{3}He born in the solid. The effects of ^{3}He cannot be ignored in DT layers that have aged for longer than ~1 day.
5. C. Y. Kuo, R. J. Kerl, N. D. Patel, and C. K. N. Patel, *Phys. Rev. Lett*. **53**, 2575 (1984).
6. H. P. Gush, W. F. J. Hare, E. J. Allin, and J. L. Welsh, *Can. J. Phys*. **38**, 176 (1960).
7. G. W. Collins et al., *J. Vac. Sci. Technol. A* **14**(5), 2897 (1996).
8. R. B. Stephens and G. Collins, *Fusion Technol*. **31**, 485 (1997).
9. Infragold™ is an electrochemically plated, diffuse, gold-metallic coating. For information, contact Labsphere, North Sutton, NH, 03260.
10. *General Atomics Inertial Confinement Fusion Annual Report*, General Atomics report GA-A22816, UC-712, 5–7 (1997).
11. Ray tracing was performed using the TracePro™ commercial optical modeling program. For further information, contact Lambda Research Corp., Littleton, MA 01460.
12. After pyrolysis, the shells were inspected and measured using a microscope calibrated using a 1-mm-diam reference sphere.
13. E. R. Mapoles, J. Sater, J. Pipes, and E. Monsler, *Phys. Rev. E* **55**, 3473 (1997).
14. P. C. Souers, *Hydrogen Properties for Fusion Energy* (University of California Press, Berkeley, CA, 1986), p. 61.
15. B. J. Kozioziemski, G. W. Collins, and T. P. Bernat, *Fusion Technology* **31**, 482 (1997).
16. W. W. Mullins, *J. App. Phys*. **28**, 333 (1957).
17. DT experiences a 12% shrinkage when cooling through the triple point. Thus, a 1-mm capsule full of liquid at just above the triple point would have a uniform solid layer 253-μm thick just below the triple point temperature.